ACS APPLIED MATERIALS & INTERFACES

Research Article

www.acsami.org

Functionalized Collagen Scaffold Neutralizing the Myelin-Inhibitory Molecules Promoted Neurites Outgrowth in Vitro and Facilitated Spinal Cord Regeneration in Vivo

Xing Li,[†,§,∥] Jin Han,[†,∥] Yannan Zhao,[†] Wenyong Ding,[‡] Jianshu Wei,[†] Sufang Han,[†] Xianping Shang,[‡] Bin Wang,[†] Bing Chen,[†] Zhifeng Xiao,[†] and Jianwu Dai*[,†]

[†]State Key Laboratory of Molecular Developmental Biology, Institute of Genetics and Developmental Biology, Chinese Academy of Sciences, Beijing 100101, China

[‡]Department of Biochemistry, Dalian Medical University, Dalian 116044, China

[§]University of Chinese Academy of Sciences, Beijing 100190, China

ABSTRACT: Research has demonstrated that many myelin-associated inhibitory molecules jointly contribute to the failure of adult spinal cord regeneration. Therapies comprehensively targeting the multiple inhibitory nature of the injured spinal cord are being concerned. Here, two collagen-binding proteins, CBD-EphA4LBD and CBD-PlexinB1LBD, were constructed, respectively, to neutralize the axon guidance molecules ephrinB3 and sema4D that inhibit the regeneration of nerve fibers. The two neutralizing proteins have proven their ability to specifically bind collagen and to continuously release from collagen scaffolds. They could also promote neurites outgrowth of cerebellar granular neurons and dorsal root ganglion neurons in vitro. Subsequently, the functionalized collagen scaffolds by physically absorbing NEP1-40 and immobilizing CBD-EphA4LBD and CBD-PlexinB1LBD were transplanted into a rat T10 complete spinal cord transection model. Our results showed that rats that received the treatment of transplanting the functionalized collagen scaffold exhibited great advantage on axonal regeneration and locomotion recovery after spinal cord injury.

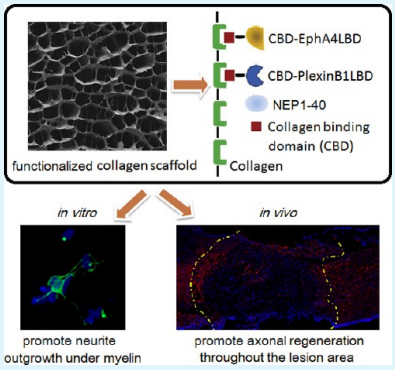

KEYWORDS: *spinal cord injury, neutralizing protein, functionalized collagen scaffold, collagen binding domain, myelin-inhibitory molecules*

1. INTRODUCTION

Spinal cord injury (SCI) is usually followed by loss of sensation and voluntary movements below the level of lesion.[1] Unlike neonatal or peripheral neurons that could regenerate after injury, the adult mammalian central nervous system (CNS) neurons generally are incapable of spontaneously regenerating into or passing through the lesion site.[2] Decades of research have demonstrated that the regeneration failure of mature CNS axons is attributed to several mechanisms.[2−4] Among them, myelin-associated inhibitors (MAIs) have been identified as one of the chief culprits to prevent the regeneration of adult CNS neurons.[5] Nogo, myelin-associated glycoprotein (MAG), and oligodendrocyte myelin glycoprotein (OMgp) as main candidates of myelin-associated inhibitory molecules have been paid great attention for decades, and the research on them is fairly deep and specific.[6−8] The strategies aiming to attenuate the inhibition of MAIs included administrating of small antagonist peptides (such as NEP1-40) or modified receptors (such as NgR-Fc), and such strategies have been proven to be successful in promoting regeneration of nerve fibers and recovery of locomotor function.[6−8]

Besides MAIs, several members of the axon guidance molecules expressed by oligodendrocytes have also been implicated to play adverse roles in CNS axon regeneration, such as ephrinB3 and semaphorin4D (sema4D). EphrinB3 was highly expressed in CNS myelin and acted as a strong inhibitor to neurite outgrowth for postnatal cortical neurons in vitro.[9] In vivo, ephrinB3 restricted axonal regeneration and functional recovery after adult CNS injury.[10] The receptor of ephrinB3 was identified to be EphA4, which accumulated in severed corticospinal tract axons of spinal cord injured rats.[11] Moreover, the EphA4 null mice exhibited better axonal regeneration and locomotion recovery after spinal cord hemisection than the wild-type ones.[12] Sema4D, which was overexpressed in oligodendrocyte precursor cells (OPCs) near sites of the injured spinal cord, has also been validated to inhibit outgrowth of postnatal cerebellar and sensory neurites in vitro.[13] Few repair strategies by blocking sema4D signaling have been reported until recently Zhang et al. indicated that SCI rats with sema4D knockdown in oligodendrocytes showed promoted functional recovery, which indicated that blocking sema4D could be a potential strategy for SCI treatment.[14] However, independently targeting a single inhibitor could only lead to modest or limited axonal regrowth (sprout) into the lesion

Received: April 2, 2015
Accepted: June 2, 2015
Published: June 2, 2015

DOI: 10.1021/acsami.5b03879
ACS Appl. Mater. Interfaces 2015, 7, 13960−13971

site.[15] Therefore, investigating combinatorial therapies comprehensively dealing with the potential inhibitors is of great significance.

Benefitting from low antigenicity, excellent biocompatibility, and good biodegradability when implanted in vivo, collagen is widely used as one of the most popular biomaterials for spinal cord regeneration.[16−18] In our previous studies, neurotrophic factors modified with a collagen binding domain (CBD) further enable collagen scaffolds to be an excellent drug sustained-releasing carrier.[16−19] In this study, a well-organized linear porous collagen scaffold was developed to support axonal attachment and to bridge axonal regeneration. In addition, both the ligand binding domains (LBDs) of the receptors of ephrinB3 and sema4D were, respectively, fused with a CBD to create the recombinant proteins possessing a special binding ability to collagen. The recombinant proteins blocked the inhibitory activity of CNS myelin and promoted neurite outgrowth in vitro. Then, a functionalized collagen biomaterial was developed by combining the linear porous collagen scaffold, collagen-binding recombinant proteins, and NEP1-40, aiming to neutralize the known axonal regeneration inhibitors. The functionalized collagen scaffold was transplanted into the injury site of a rat spinal cord T10 completed transverse model. We are trying to find a combinatorial but feasible treatment program in order to reconstruct the complicated system and finally have the potential in clinical application. Our findings indicated that the combinatorial therapy could effectively facilitate axonal regeneration and locomotion recovery after spinal cord injury.

2. EXPERIMENTAL METHODS

2.1. Protein Expression, Purification, and Homology Modeling. EphA4-LBD and PlexinB1-LBD were composed of peptides consisting in the extracellular LBD of human EphA4 (amino acids 4−179) and human PlexinB1 (amino acids 73−215), respectively. The cDNA sequences of EphA4-LBD and PlexinB1-LBD were then separately cloned into pET-28a and pET-CBD, and the two plasmids were constructed as describe previously.[16,19] After sequence confirmation, the plasmids were transformed into *Escherichia coli* strain BL21 (DE3) competent cells for protein expression. *E. coli* cells were cultured in LB medium supplied with 50 mg/L kanamycin at 37 °C. When the OD_{600} of the cultures reached 0.8, 1 mM isopropyl β-D-1-thiogalactopyranoside (IPTG) was added, and the cultures were incubated for another 4 h at 25 °C. The cells were harvested by centrifugation, resuspended in 10 mL of 0.05 M sodium phosphate buffer (pH 7.5) containing 5 mM imidazole, and then, sonicated on ice for 5 min at 50% pulses using an Ultrasonic Crasher (Ningbo Scientz Biotechnology Co., Ltd., China). The homogenate was centrifuged for 10 min at 10 000*g* and 4 °C. The His-tagged protein was isolated through a prepacked 5 mL Hi-trap Ni column (Pharmacia, USA) following the manufacturer's protocol. The purified recombinant protein was stored at −80 °C until use. The efficiency of purification was monitored by sodium dodecyl sulfate polyacrylamide gel electrophoresis (SDS-PAGE). Protein concentration was determined by the Bradford method with bovine serum albumin (BSA) as the standard.

The models of EphA4-LBD and PlexinB1-LBD interacted with each of their ligands were generated by the SWISS-MODEL Workspace (http://swissmodel.expasy.org/workspace/) based on the crystal structure of the Eph receptor with ephrin (PDB ID: 3GXU) and sema4D with Plexin B1 (PDB ID: 3OL2) from human. The three-dimensional (3D) figure was prepared with the program PyMOL (http://www.pymol.org; DeLano Scientific, USA).

2.2. Myelin Preparation. Myelin isolated from adult rat was in accordance with a previous report in our lab.[20] To isolate myelin, tissue is homogenized in 0.3 M sucrose and layered on a gradient of 1.23 and 0.85 M sucrose. Samples are centrifuged for 45 min at 75 000*g*, and the crude myelin fraction is collected at the 0.85/1.23 M interface. Crude myelin is washed twice by osmotic shock, resuspended in 0.32 M sucrose, layered over 0.85 M sucrose, centrifuged, and collected from the 0.32/0.85 M interfaces. After removal of excess sucrose, myelin is resuspended 1:1 in DMEM, homogenized, and stored at −80 °C until use.

2.3. Preparation of Collagen Scaffold and Scanning Electron Microscopy Characterization. Collagen scaffolds were fabricated as described previously with modification.[21] Briefly, the collagen membranes were immersed in 0.5 M acetic acid solution for 8 h at 4 °C. Then, the solution was mixed in a blender for 15 min to obtain a homogeneous collagen solution and neutralized by 4 M NaOH. The homogeneous solution was dialyzed in deionized water for 5 days and lyophilized. The obtained porous collagen scaffolds were cut into 0.2 × 0.5 × 0.5 cm^3 pellets, and the solid pellets were immersed in 40 mL of MES (pH 6.5) containing 1 mg/mL 1-ethyl-3-(3-dimethyl aminopropyl) carbodiimide and 0.6 mg/mL *N*-hydroxysuccinimide at 37 °C for 4 h. After cross-linking, the pellets were successively washed by 4 M NaCl and ddH_2O at 37 °C for 1 h before being lyophilized again. Then, the pellets were sterilized by Co 60 and stored at 4 °C for utilization. As we have reported previously, both the hardness and elasticity of the collagen scaffold are increased after cross-linking.

For scanning electron microscopy (SEM), the scaffolds were fixed in 2% glutaraldehyde for 40 min at 4 °C. Subsequently, they were dehydrated in ethanol with a series of concentrations: 30%, 50%, 70%, 75%, 80%, 85%, 90%, and 95% for 10 min, and 100% for 20 min. The ethanol was extracted in 3:1, 1:1, and 1:3 mixtures of ethanol and amyl acetate for 20 min each followed by 100% amyl acetate storage for 20 min. Then, the samples were dried by super critical CO_2 extraction and coated with gold using a sputter. The images were captured by a HITACHI S-3000N scanning electron microscope (Hitachi, Japan).

2.4. Binding Assay of CBD-EphA4-LBD and CBD-PlexinB1-LBD to Collagen. The binding ability of CBD-EphA4-LBD and CBD-PlexinB1-LBD to collagen was measured by a modified enzyme-linked immunosorbent assay (ELISA) according to our previous report.[19] The type I collagen prepared from rat tail tendon was added to a 96-well plate, and the plate was blocked with fetal bovine serum for 2 h at room temperature (rt). Serial dilutions of CBD-EphA4-LBD and CBD-PlexinB1-LBD were added to the wells and incubated at 37 °C for 2 h; then, unbound proteins were removed by washing extensively with phosphate-buffered saline (PBS). Antipolyhistidine monoclonal antibody (Sigma−Aldrich, USA) was used as the primary antibody, and alkaline phosphatase (ALP)-conjugated goat-antimouse IgG (Sigma−Aldrich) was used as the secondary antibody. The remaining proteins were detected by 2 mg/mL *p*-nitrophenylphosphate (Sigma−Aldrich) in ALP buffer (100 mM Tris−HCl, 100 mM NaCl, and 10 mM $MgCl_2$, pH 9.6) for 30 min at 37 °C. The results were quantified at 405 nm using an ELISA reader (Molecular Devices, USA). A calibration curve was constructed for each sample to quantitate the total amounts of proteins retained by the collagen. The results were analyzed on a Scatchard plot, and the K_d of each protein was determined using the least-squares method.

2.5. Sustained Release Assay from Collagen Scaffold. Collagen scaffolds (4 mm in diameter and 1 mm in thickness) were loaded with 5 μg of CBD-EphA4-LBD, EphA4-LBD, CBD-PlexinB1-LBD, or PlexinB1-LBD, respectively, and then placed in a 48-well plate. Briefly, 5 μg of CBD-EphA4-LBD and/or 5 μg of CBD-PlexinB1-LBD or 5 μg the non-CBD-fused counterparts were dissolved in 20 μL of PBS. Then, the 20 μL solution was added to the dry scaffold to make it fully absorbed. After incubating for 30 min at rt, the scaffolds were used for the release assay. The scaffolds were suspended in 500 μL of PBS and incubated on a rocker platform (37 °C, 80 rpm). The PBS in the 48-well plate was changed every 12 h. Samples were collected at each time point, and the proteins retained on the scaffolds were analyzed by ELISA.

2.6. Cerebellar Granular Neuron Isolation, Culture, and Neurite Outgrowth Assay. Cerebellar granular neurons (CGNs) were isolated from the postnatal rat cerebellum, and the procedures of isolation and culture were as previously described.[22] For assays of

DOI: 10.1021/acsami.5b03879
ACS Appl. Mater. Interfaces 2015, 7, 13960−13971

neurite outgrowth on myelin, ephrinB3-Fc, or sema4D-Fc substrates, 48-well plates were coated with 100 g/mL poly-L-lysine and washed, and then, 30 μL of PBS containing 0, 20, 400, or 600 ng of myelin, or 200 ng of ephrinB3-Fc or sema4D-Fc with various amount of CBD-EphA4-LBD, CBD-PlexinB1-LBD, or NEP1-40 were spotted before addition of dissociated CGNs. The cells were incubated for 20 h before assessing neurite outgrowth. After being fixed by 4% formaldehydum polymerizatum (Merck, USA), the cells were immunostained for the neuronal marker βIII-tubulin (1:500; Invitrogen, USA) overnight at 4 °C and then incubated with the Alexa 488 fluorophore-conjugated secondary antibody (Invitrogen) for 1 h at rt. Hoechst33342 (1 mg/mL) dye was used to stain the nucleus DNA, and the respective images were captured with a Zeiss Axiovert 200 (Carl Zeiss, USA). Six random fields per well from three replicated wells were counted. The neurite length was measured by HCA-Vision software (Neurite Analysis Module V1.0.1, CSIRO Mathematical and Information Sciences, Australia). The data were analyzed by one-way analysis of variance (ANOVA) followed by Tukey's postcomparison analysis and presented as mean ± standard error of the mean (sem).

2.7. Dorsal Root Ganglia Isolation, Culture, and Neurite Outgrowth Assay. E15 rat dorsal root ganglia (DRG) cells were utilized for detecting the biological activity of the CBD-EphA4-LBD/CBD-PlexinB1-LBD. DRG cells were obtained and cultured as previously reported.[23] DRG cells were isolated from E15 rat embryos and digested with 0.08% trypsin (Invitrogen) for 15 min. After that, 105 cells/well were cultured in serum-free DMEM/F12 medium (HyClone, USA), supplemented with N2 (Sigma–Aldrich) in polylysine-coated 48-well plates (Costar; Corning, USA). The cells were incubated for 20 h before assessing neurite outgrowth. After being fixed by 4% formaldehydum polymerizatum (Merck), the cells were immunostained for the neuronal marker βIII-tubulin (1:500; Invitrogen) overnight at 4 °C and then incubated with the Alexa 488 fluorophore-conjugated secondary antibody (Invitrogen) for 1 h at rt. Hoechst33342 (1 mg/mL) dye was used to stain the nucleus DNA, and the respective images were captured with a Zeiss Axiovert 200 (Carl Zeiss). Six random fields per well from three replicated wells were counted. The neurite length was measured by HCA-Vision software (Neurite Analysis Module V1.0.1, CSIRO Mathematical and Information Sciences). The data were analyzed by one-way ANOVA followed by Tukey's postcomparison analysis and presented as mean ± sem.

2.8. Quantitative Polymerase Chain Reaction. Total RNA was extracted by Trizol reagent (Invitrogen) from cell cultures of CGNs when cultured for the time indicated in the experiment. A 1 mg amount of total RNA was reverse-transcribed with Superscript III (Invitrogen) after digestion by DNase I (Invitrogen) according to the manufacturer's instruction. Quantitative real-time polymerase chain reaction (qPCR) was performed by an ABI 7900HT fast real-time PCR system (Applied Biosystems, Life Technologies, USA) and SYBR Green Master Mix (Applied Biosystems) as described by the manufacturers' instructions. Briefly, 0.5 mL of cDNA mixed with 0.5 mL of primer mixture, 5 mL of Master Mix, and 4 mL of distilled water was denatured at 95 °C for 10 min followed by 40 cycles of PCR (95 °C for 15 s, 60 °C for 1 min). The sequences of the primers of RhoA were as follows: forward primer 5′-GAATG ATGAG CACAC AAGGC-3′ and reverse primer 5′-CCAAA AGCGC CAATC CTGT-3′.

Relative quantitation of the expression level was analyzed by using the $2^{-\Delta\Delta Ct}$ method. The ΔCt value resulted from the normalization β-actin Ct value, and the ΔΔCt value resulted from the normalization by the Δ Ct value.

2.9. Surgery and Tissue Processing. Experiments were performed in accordance with the Guide for the Care and Use of Laboratory Animals from the National Institutes of Health. A total of 63 adult female Sprague Dawley rats (200–250 g) were housed in temperature- and humidity-controlled animal quarters with a 12 h light/dark cycle.

The surgery procedure was slightly modified according to our previous report.[17] Following intraperitoneal anesthesia with sodium pentobarbital (50 mg/kg), a 2 cm midline incision was made to expose the T9–T12 vertebrae. A 2 mm long transected laminectomy in T9–T10 was performed using a no. 11 blade under observation in a microscope. The transaction site was irrigated with normal saline, and bleeding was controlled using cotton-tipped applicators. Following treatment, the musculature and skin were closed in separate layers with sutures, after which the animals were returned to their home cage to recover.

All animals were randomly divided into five groups accepting different treatments. Group 1 was a blank control that received no treatment after injury (n = 12); group 2 received only transplantation of the collagen scaffold (n = 12); groups 3 and 4 received the collagen scaffold combined with 3 μg of single CBD-EphA4-LBD or CBD-PlexinB1-LBD, separately (n = 12); and group 5 that was designed to neutralize the MAIs received the collagen scaffold combined with 3 μg of CBD-EphA4-LBD, 3 μg of CBD-PlexinB1-LBD, and 0.7 μg of NEP1-40 (n = 15). The numbers of rats that survived by the end of the experiment in each group were 6, 7, 8, 7, and 10, respectively.

2.10. Histology and Immunolabeling. Twelve weeks after lesions, animals were transcardially perfused with 4% paraformaldehyde in 0.1 M phosphate buffer (pH 7.2). The spinal cord cords were dissected, postfixed overnight at 4 °C, and transferred to 20% sucrose (overnight at 4 °C) and then 30% sucrose (72 h at 4 °C). A 1–1.5 cm length of spinal cord was sectioned horizontally through its dorsal-to-ventral axis on a cryostat set at 10 μm thickness; the center of the block corresponded to the center of the lesion site. For immunocytochemistry, the slides were fixed in acetone for 15 min at 4 °C, and then, the samples were incubated in PBS containing 5% BSA with 0.1% Trition X-100 for 1 h at rt. The samples were incubated with primary antibodies anti-GFAP (1:800; Invitrogen), anti-neurofilament (NF, 1:200; Abcam, USA), anti-S100 (1:500; Abcam), and anti-serotonin (5-HT) (1:10 000; polyclonal from ImmunoStar, USA) overnight at 4 °C and then incubated in Alexa 488 conjugated donkey antirabbit secondary antibody (1:500, A21206, Invitrogen) and Alexa 594 conjugated donkey antimouse secondary antibody (1:800, A21203; Invitrogen) for 1 h at rt. Hoechst33342 (1 mg/mL) dye was used for nuclear staining. To evaluate the density of NF-positive nerve fibers and 5-HT-positive neurons, the nerve fiber numbers or neurons were counted per field in six random areas of the rostral border, caudal border, and the lesion center of samples.

2.11. Functional Analysis. Locomotion recovery after SCI was scored according to the BBB open field 21 point locomotion rating scale.[24] Animals were allowed to assess the movements of hindlimbs weekly by two independent observers blinded to the treatments identity.

2.12. Statistical Analysis. The data are presented as mean ± standard deviation. Multiple group comparisons were made using one-way ANOVA. Two-group comparisons were tested by Student's test. * represented a p value < 0.05, and ** represented a p value < 0.01.

3. RESULTS

3.1. Molecular Cloning, Modification, Purification, and Homology Modeling of the Ligand Binding Domain of EphA4 and PlexinB1. The LBD of human EphA4, the receptor of myelin-associated axon guidance molecule ephrinB3, was cloned and inserted into pET-CBD and pET-28a to construct the expression vectors for recombinant proteins with or without the CBD. The pET-CBD vector was constructed as previously described.[16] Additionally, we also cloned part of the LBD sequence of human PlexinB1, the receptor of another axon guidance molecule named sema4D, and then constructed it into the pET-CBD vector to form pET-CBD-PlexinB1-LBD. The deduced amino acid sequences of the LBDs of EphA4 and PlexinB1 showed that residues responsible for ligand binding were conserved across various species (comparison result was not shown). Residues not fully conserved were found distant from the ligand binding and interfering residues in the predicted 3D structure of EphA4-

DOI: 10.1021/acsami.5b03879
ACS Appl. Mater. Interfaces 2015, 7, 13960–13971

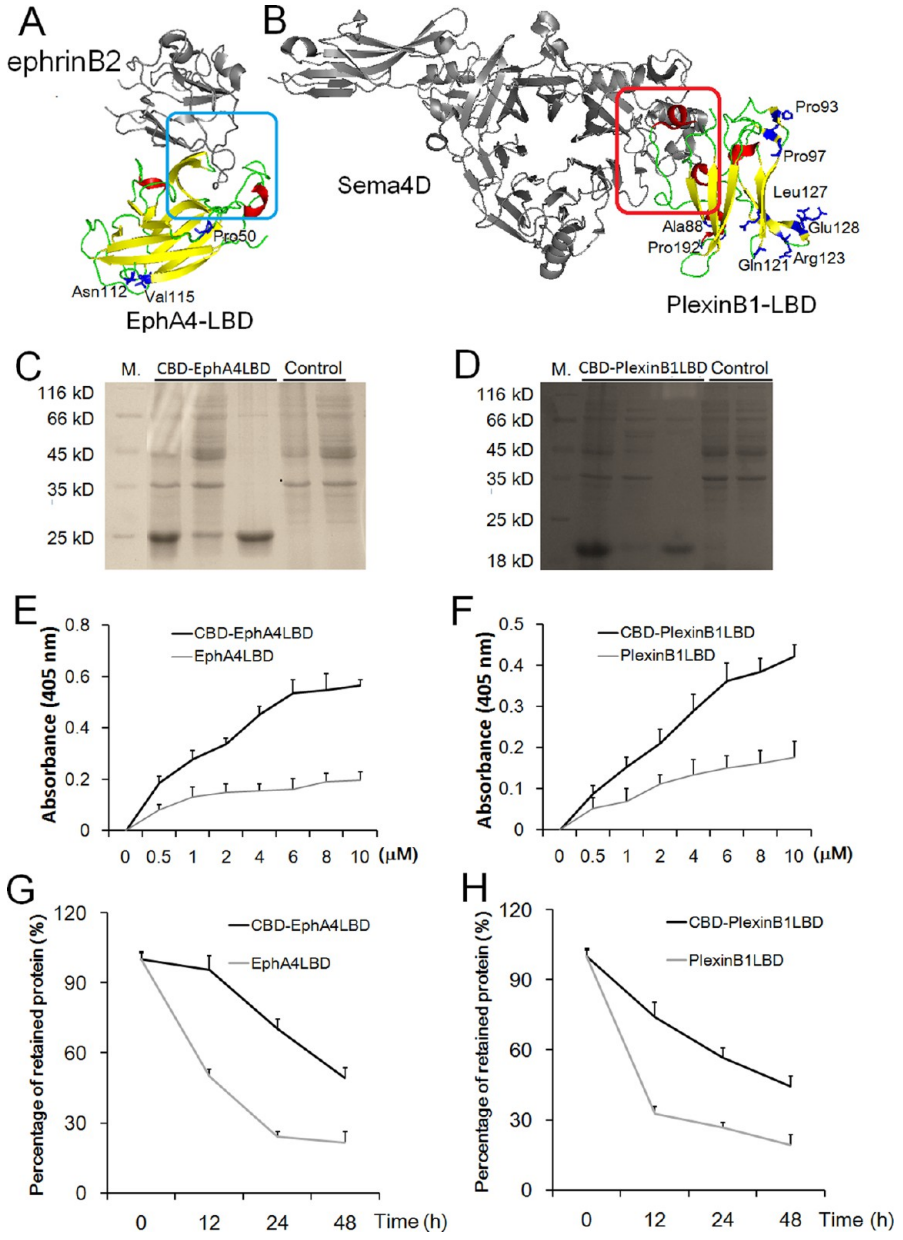

Figure 1. Modeling, purification, and characterization of CBD-EphA4-LBD and CBD-PlexinB1-LBD. Homology models of (A) human EphA4-LBD interacting with ephrinB2 and (B) human PlexinB1-LBD interacting with sema4D. The blue and red boxes represent the receptor−ligand interactive region. Residues in human EphA4-LBD and PlexinB1-LBD that differ from those in rat are shown in sticks with blue labels. (C, D) Coomassie blue stained SDS-PAGE under reduced condition of CBD-EphA4-LBD and CBD-PlexinB1-LBD: M, molecular weight markers; lanes 2−3, crude extract, total soluble proteins of *E. coli* BL21 induced by IPTG; lane 4, the purified protein; lanes 5−6 (control), crude extract (lane 5) and total soluble proteins (lane 6) of *E. coli* BL21with the empty plasmid induced by IPTG. (E) Binding curves of EphA4-LBD and CBD-EphA4-LBD to collagen in vitro. (F) Binding curves of PlexinB1-LBD and CBD-PlexinB1-LBD to collagen in vitro. (G) Release assay of EphA4-LBD and CBD-EphA4-LBD from the collagen scaffold. (H) Release assay of PlexinB1-LBD and CBD-PlexinB1-LBD from the collagen scaffold.

LBD and PlexinB1-LBD, respectively (Figure 1A, B). SDS-PAGE indicated that the purified CBD-EphA4-LBD and CBD-PlexinB1-LBD were successfully prepared (Figure 1C and D, respectively).

3.2. CBD-EphA4-LBD and CBD-PlexinB1-LBD Showed Specific Binding Activity of Collagen and Could be Sustained Released from the Collagen Scaffold. The collagen-binding abilities of CBD-EphA4-LBD and CBD-PlexinB1-LBD were assessed by ELISA. By comparing the optical density at 405 nm, the amounts of retained CBD-EphA4-LBD and CBD-PlexinB1-LBD on the collagen were significantly higher than those of EphA4-LBD and PlexinB1-LBD, respectively, at solution concentrations ranging 0.5−10 μM (Figure 1E, F). The amounts of retained CBD-EphA4-LBD and CBD-PlexinB1-LBD were calculated by Scatchard analysis based on the standard curve. The K_d values for the binding of CBD-EphA4-LBD and CBD-PlexinB1-LBD to collagen were 0.43 and 0.36 μM, respectively. The K_d values of the two recombinant proteins were close to those of CBD-BDNF (0.42 μM) and CBD-NT3 (0.35 μM) calculated in our previous research that indicated that these CBD-fused proteins shared a similar collagen-binding ability.[16,17]

In addition, differential sustained release of CBD-EphA4-LBD and CBD-PlexinB1-LBD with their own non-CBD-fused

DOI: 10.1021/acsami.5b03879
ACS Appl. Mater. Interfaces 2015, 7, 13960−13971

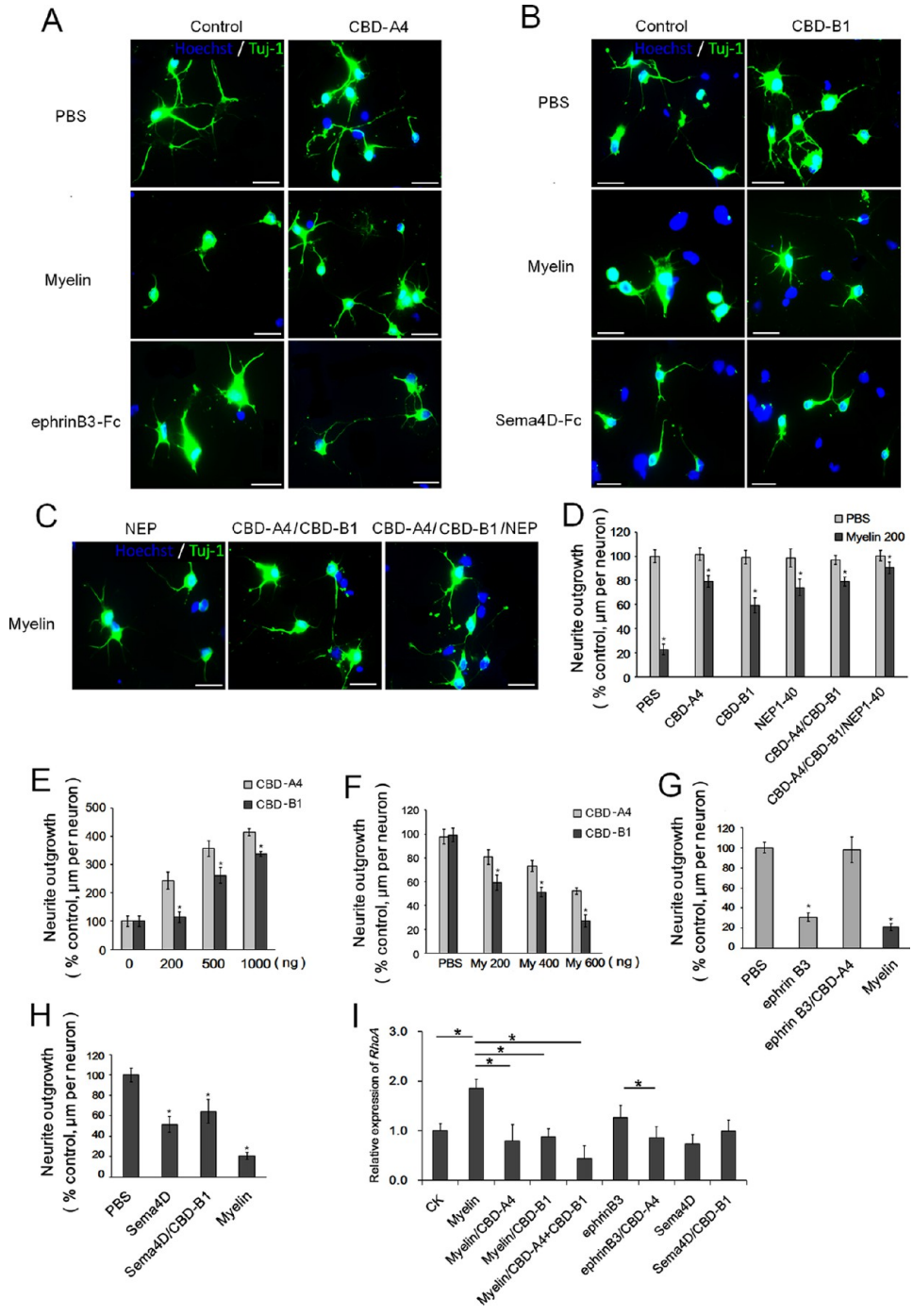

Figure 2. Neurite outgrowth of CGNs on myelin substrates can be promoted by addition of CBD-EphA4-LBD and CBD-PlexinB1-LBD. (A) Inhibition of myelin or ephrinB3-Fc on CGN neurite outgrowth was partially reversed by the addition of CBD-EphA4-LBD. (B) Inhibition of myelin or sema4D-Fc on CGN neurite outgrowth was slightly reversed by the addition of CBD-PlexinB1-LBD. (C) CBD-EphA4-LBD, CBD-PlexinB1-LBD, and NEP1-40 showed the synergetic effect on promoting CGN neurite outgrowth in the presence of myelin. (D) Quantification of CBD-EphA4-LBD, CBD-PlexinB1-LBD, NEP1-40, and their combination on CGN neurite outgrowth in the presence or absence of 200 ng of myelin. (E) In the presence of 200 ng of myelin, CGN neurite outgrowth could be detected in a dose-response manner when 0, 200, 500, or 1000 ng of CBD-EphA4-LBD or CBD-PlexinB1-LBD was added. (F) CGN neurite outgrowth on 0, 200, 500, or 1000 ng of myelin was tested when treated with 200 ng of CBD-EphA4-LBD or CBD-PlexinB1-LBD. (G) Quantification of neurite outgrowth indicated that CBD-EphA4-LBD addition can attenuate the inhibition of both ephrinB3-Fc and myelin. (H) Quantification of neurite outgrowth indicated that CBD-PlexinB1-LBD addition can promote neurite outgrowth in the presence of sema4D or myelin. (I) qPCR for RhoA gene expression of cultured CGNs. The CGNs were pretreated with PBS, 200 ng of myelin, ephrinB3-Fc, or sema4D-Fc. After adding with or without CBD-EphA4-LBD or CBD-PlexinB1-LBD, cell samples were collected for qPCR assays. (*$p < 0.05$, determined by Student's t test) . CGNs were stained with a Tuj-1 antibody (green) and Hoechst for nuclei (blue). In A–C, the scale bar = 50 μm. CBD-A4, CBD-B1, NEP, and My represent CBD-EphA4-LBD, CBD-PlexinB1-LBD, NEP 1-40, and myelin, respectively.

DOI: 10.1021/acsami.5b03879
ACS Appl. Mater. Interfaces 2015, 7, 13960–13971

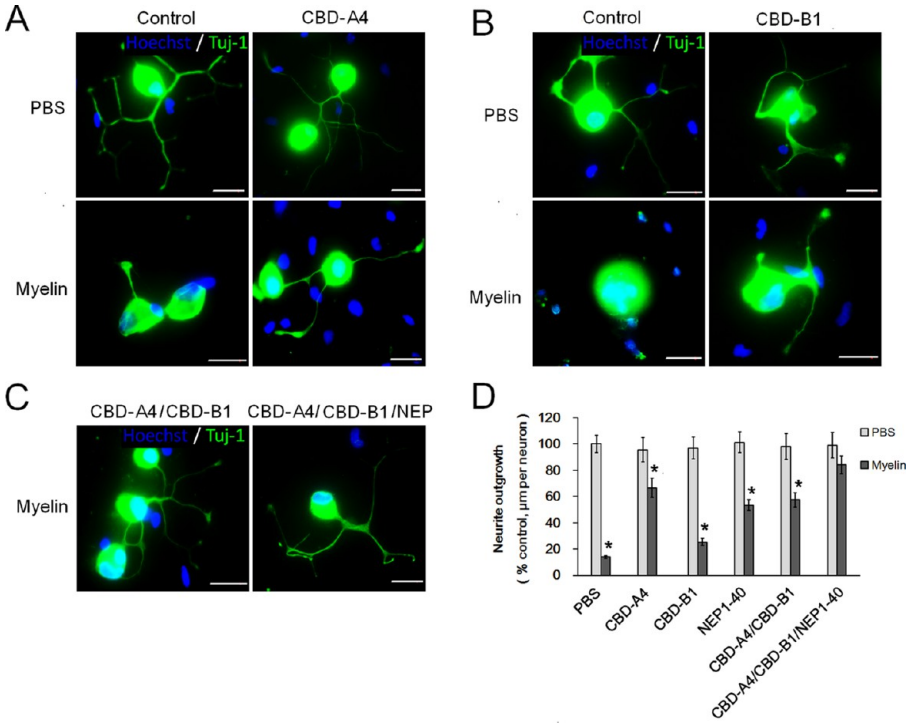

Figure 3. CBD-EphA4-LBD and CBD-PlexinB1-LBD can antagonize the inhibition of myelin substrates on neurite outgrowth of DRG. (A, B) Dissociated DRG cultured on 48-well plates were pretreated with PBS or 200 ng of myelin. After the addition with (A) CBD-EphA4-LBD or (B) CBD-PlexinB1-LBD, the myelin inhibition effect on neurite outgrowth of DRG was partially reversed. (C) CBD-EphA4-LBD, CBD-PlexinB1-LBD, and NEP1-40 showed the synergetic effect on promoting DRG neurite outgrowth in the presence of myelin. (D) Quantification of CBD-EphA4-LBD, CBD-PlexinB1-LBD, NEP1-40, and their combination on DRG neurite outgrowth in the presence or absence of 200 ng of myelin. DRG were stained with a Tuj-1 antibody (green) and Hoechst for nuclei (blue). $*p < 0.05$, determined by Student's t test. CBD-A4, CBD-B1, and NEP represent CBD-EphA4-LBD, CBD-PlexinB1-LBD, and NEP 1-40, respectively.

counterparts was observed for 48 h. From the results, we found that EphA4-LBD and PlexinB1-LBD were quickly released from the porous collagen scaffold in the first 6 h, whereas CBD-EphA4-LBD and CBD-PlexinB1-LBD could gradually release from collagen during the observed period. The differences between CBD-fused proteins and their non-CBD-fused counterparts released from the collagen scaffold were significant during the whole 48 h (Figure 1G, H). The results above suggest that CBD-fused proteins possess specific collagen binding activity and the binding ability made them release from the collagen scaffold more slowly and constantly.

3.3. Recombinant CBD-EphA4-LBD and CBD-PlexinB1-LBD Could Partially Block the Inhibitory Effect of CNS Myelin and Promote Neurite Outgrowth in Vitro. After confirming the binding ability of CBD-EphA4-LBD and CBD-PlexinB1-LBD to collagen, we then investigated the influences of the two CBD-fused proteins on neurite outgrowth of cultured neurons. We carried out CGN and DRG neurite outgrowth assays to verify whether the recombinant CBD-EphA4-LBD and CBD-PlexinB1-LBD could block inhibitory activity of CNS myelin. Results showed that, when dissociated rat CGNs or DRG plated on PBS, myelin, or ephrinB3 were treated with 200 ng of soluble recombinant CBD-EphA4-LBD, the inhibitory effect of myelin and ephrinB3 on neurite outgrowth was attenuated by CBD-EphA4-LBD addition (Figures 2 and 3). Furthermore, in the absence of myelin, the addition of recombinant CBD-EphA4-LBD did not inhibit neurite outgrowth (Figures 2D and 3D). The antagonist effect of CBD-PlexinB1-LBD against myelin or sema4D by CGN or DRG neurite outgrowth assays could also be detected (Figures 2B and 3B). However, the role of CBD-PlexinB1 on promoting neurite outgrowth was not as dramatic as what CBD-EphA4-LBD exhibited (Figure 2D, E). Moreover, in the presence of myelin, both CBD-EphA4-LBD and CBD-PlexinB1-LBD could promote neurite outgrowth in a dose-dependent manner up to 1000 ng (Figure 2E). Likewise, in the presence of CBD-EphA4-LBD or CBD-PlexinB1-LBD, the prevention of CGN neurite outgrowth by myelin also presented a dose-dependent manner (Figure 2F). In addition, the synergetic effect of CBD-EphA4-LBD, CBD-PlexinB1-LBD, and NEP1-40 on promoting CGN neurite outgrowth could be evidently observed (Figure 2D). The independent and synergetic effects of CBD-EphA4-LBD, CBD-PlexinB1-LBD, and NEP1-40 on promoting DRG neurite outgrowth were also tested, and the results were similar to those obtained from CGN neurite outgrowth assays (Figure 3D). The effect of CBD-EphA4-LBD or CBD-PlexinB1 on promoting neurite outgrowth in vitro showed no significant differences with their non-CBD-fused counterparts (data not shown).

By analyzing the gene expression profile of endogenous RhoA in cultured CGNs, we found that, when myelin was added in the medium, the expression level of RhoA was increased. After the recombinant CBD-EphA4-LBD was added in the myelin-pretreated medium, the expression level of RhoA decreased (Figure 2I). In addition, when treated with ephrinB3-Fc, the expression level of RhoA was found to be slightly increased. Moreover, when both ephrinB3-Fc and CBD-EphA4-LBD were added in the medium, the expression level of RhoA lowered (Figure 2I). Our study also substantiated the effect of CBD-PlexinB1-LBD in promoting CGN neurite

DOI: 10.1021/acsami.5b03879
ACS Appl. Mater. Interfaces 2015, 7, 13960−13971

outgrowth (Figure 2D, E, H). The upregulation of RhoA by myelin was also attenuated by the addition of CBD-PlexinB1-LBD (Figure 2I). In addition, the synergetic effects of CBD-EphA4-LBD, CBD-PlexinB1-LBD, and NEP1-40 on decreasing RhoA expression was also observed (Figure 2I).

Except for CGN neurite outgrowth assays carried out on traditional two-dimensional culture, the dissociated CGNs were also seeded in functionalized collagen scaffolds modified with CBD-EphA4-LBD or CBD-PlexinB1-LBD. The neurite outgrowth inhibition of myelin added in the culture medium was also shown to be partially blocked by the immobilized 200 ng of CBD-EphA4-LBD or CBD-PlexinB1-LBD on the surface of the functionalized scaffolds (Figure 4).

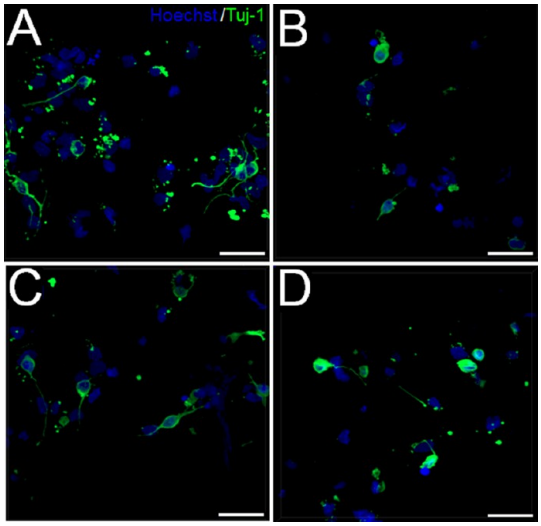

Figure 4. CGN neurite outgrowth could be promoted in the presence of myelin when cells were cultured on a collagen scaffold immobilized with CBD-EphA4-LBD or CBD-PlexinB1-LBD. The dissociated CGNs on the 3D scaffold were treated with PBS (A), 200 ng of myelin (B), 200 ng of myelin mixed with CBD-EphA4-LBD (C) or CBD-PlexinB1-LBD (D). CBD-EphA4-LBD and CBD-PlexinB1-LBD showed their ability to partially promote CGN neurite outgrowth in the presence of myelin. CGNs were stained with a Tuj-1 antibody (green) and Hoechst for nuclei (blue).

3.4. Characterization of the Functionalized Collagen Scaffold for the Rat T10 Complete Transection Model.

The collagen scaffold fabricated in this study presented a spongelike porous structure constituted of well-organized linear pores with a diameter of 10−30 μm, and the porosity of this scaffold was more than 90% (Figure 5A), suggesting that it could be an ideal candidate to bridge across the lesion site after SCI. Figure 5A shows representative SEM images of both the transverse and longitudinal profiles of the collagen scaffold. After cross-linking and sterilization, the collagen scaffold was cut into disk-shaped pieces (4 mm in diameter, 2−3 mm in thickness) for the immobilization of CBD-fused proteins. After incubation with specific proteins for 0.5 h, the functionalized collagen scaffold was transplanted into the injured site of the rat spinal cord as a permissive matrix for axonal attachment and extension after receiving a complete T10 spinal cord transection. The scaffolds were also used in the in vitro CGN 3D culture experiments (Figure 4) and protein release assay (Figure 1) mentioned above. The cylindrical scaffold for transplantation is shown in Figure 5A.

In this study, all animals were randomly divided into five groups accepting different treatments. Group 1 (n = 12) was a blank control that received no treatment after injury; group 2 (n = 12) received only transplantation of the collagen scaffold; group 3 (n = 12) and group 4 (n = 12) received the collagen scaffold immobilized with 3 μg of single CBD-EphA4-LBD or CBD-PlexinB1-LBD, separately; group 5 (n = 15) received the functionalized collagen scaffold modified with 3 μg of CBD-EphA4-LBD, 3 μg of CBD-PlexinB1-LBD, and 0.7 μg of NEP1140 to neutralize the know MAIs ephrinB3, sema4D, and Nogo (Figure 5B).

3.5. Functionalized Collagen Scaffold Promoted Axonal Regeneration, Remyelination, and Locomotion Recovery.

As the recombinant CBD-EphA4-LBD and CBD-PlexinB1-LBD showed their ability to block the inhibitory nature of CNS myelin by promoting CGN and DRG neurite outgrowth in vitro, we further carried out a rat spinal cord injury assay to verify whether the proteins could also neutralize the MAIs in vivo when immobilized on the surface of the linear porous collagen scaffold.

In all groups, the residual axons after complete transection have been found to regenerate through the GFAP immunoreactive interfaces and to penetrate into the lesion area from both the rostral and caudal host tissues adjacent to the lesion. The axon number penetrated into the lesion area in each group was quantified, which revealed that rats received transplanting of the functional scaffolds modified by CBD-EphA4-LBD (group 3) or CBD-PlexinB1-LBD (group 4) could both promote more axon fibers penetrating into the lesion site than rats in the control (group 1) and material (group 2) groups (Figure 6N). However, rats in group 5 that received combinatorial treatment exhibited the greatest axonal regeneration across sites of complete T10 spinal cord transection compared to all other groups ($p < 0.01$; Figure 6N). Moreover, the distance of axonal regeneration in group 5 was also the longest among all the groups in this study. The regenerated axons of several animals in group 5 have been detected extensively from the rostral to the caudal border (Figure 6I). The results above indicated that, the more inhibitory molecules the treatment targeted, the better therapeutic effect would emerge. Therefore, the amount of regenerated axons in each group presented progressive improvement by the complexity of the treatment (Figure 6P). In addition, a transmission electron microscopy study of the regenerated tissues also revealed that the remyelinated nerve fibers could be detected in all groups except the blank control group (Figure 7E−H). However, the sickness of the new-formed myelin among groups 1−5 was statistically insignificantly ($p < 0.05$; Figure 7H). We also used a marker of Schwann cells antibody S100 to clearly demonstrate the existence of Schwann cells in the lesion center (Figure 7I−K), which suggested that part of the source of myelin sheath of the regenerated axons in the lesion site was derived from the peripheral nervous system. However, the positively stained cells of the control group were significantly lower than other groups (Figure 7L).

Besides the longest regenerative nerve fibers being found in the lesion area, the NF-positive fibers penetrated into the lesion area were arranged in order (Figure 6M) that indicated that the well-organized linear pores in the collagen scaffold could support and guide the regenerated nerve fibers directionally and that the functionalized collagen scaffold could be an ideal biomaterial to bridge the lesion cavity after SCI.

DOI: 10.1021/acsami.5b03879
ACS Appl. Mater. Interfaces 2015, 7, 13960−13971

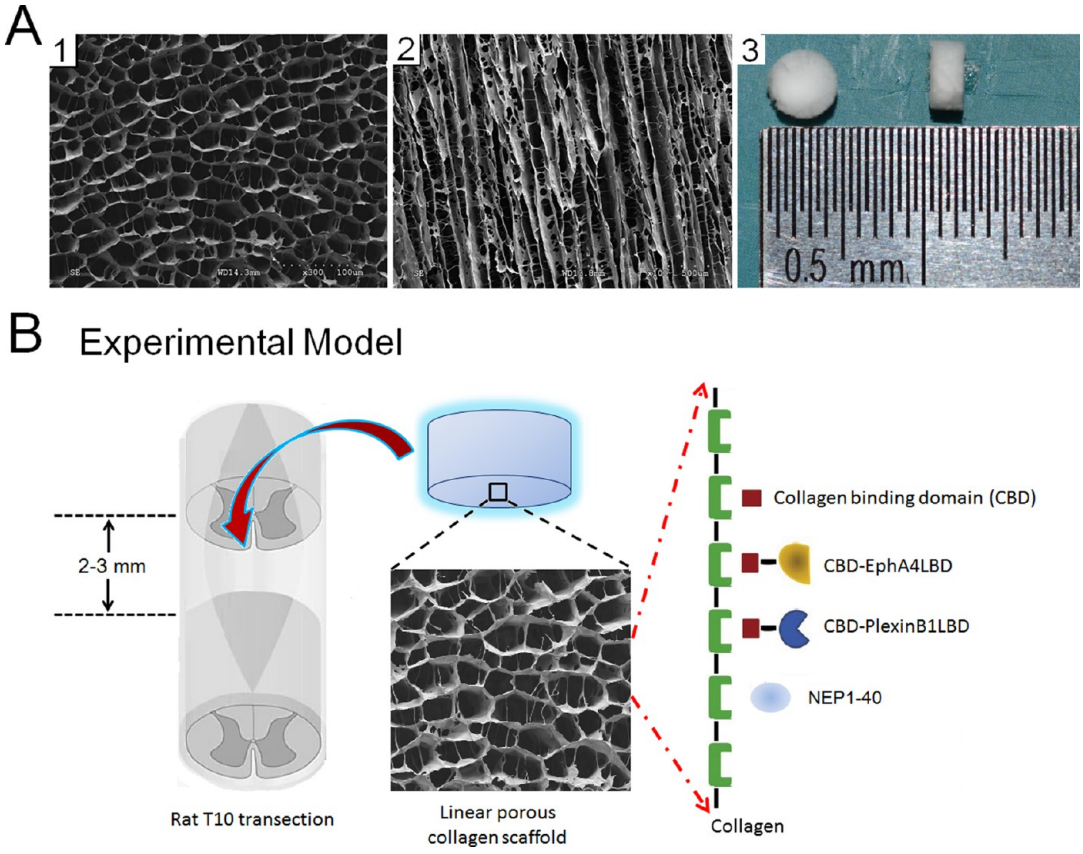

Figure 5. Collagen scaffold and the animal experiment. (A1, 2) SEM images show the transverse (A1) and longitudinal (A2) sections of the aligned collagen scaffold. (A3) Collagen scaffold with a diameter of 4 mm and a thickness of 2 mm for CGN 3D culture and spinal cord transplantation. (B) Animal experimental model was designed to carry out as follows: The collagen scaffolds were modified with NEP1-40, CBD-EphA4-LBD, and CBD-PlexinB1-LBD aiming to neutralize the inhibitory molecules Nogo, ephrinB3, and sema4D, respectively. Then, the functionalized scaffolds were transplanted into a rat T10 complete transection site.

Of note, in group 5, 5-HT-labeled axons clearly regenerated into the lesion area, and the density of the axons was much greater than that in the control groups (Figure 7A–D), which indicated that animals in group 5 that received the combinatorial treatments could promote the regeneration of serotonergic axons into the lesion site than other groups.

Locomotor outcomes were assessed on the BBB scale[24] for 12 weeks after surgery. Rats in the combinatorial treatment group exhibited significant improvements in the BBB scale compared with rats in other groups from the sixth week after surgery until killed ($p < 0.05$; Figure 8). The result suggested that the combined treatments could effectively recover the function of hindlimbs after injury.

4. DISCUSSION

As a canonical axon guidance molecule, ephrinB3 inhibits neurite outgrowth through an EphA4-dependent manner that induces growth cone collapse by activating the Rho GTPase RhoA (Figure 9).[25] The results of both neurite outgrowth assays and the gene expression profile of endogenous RhoA in cultured CGNs have indicated that RhoA activation was the principal downstream inhibitory signaling of neurite outgrowth launched by ephrinB3. The inhibitory events could be effectively attenuated by exogenous application of CBD-EphA4-LBD (Figure 2). Furthermore, plexinB1-mediated signal transduction was also proven to result in RhoA activation, and exogenous application of CBD-PlexinB1-LBD could promote neurite outgrowth of cultures CGNs under CNS myelin (Figure 2). In summary, the three neutralizing proteins CBD-EphA4-LBD, CBD-PlexinB1-LBD, and NEP1-40 were successfully observed to promote neurite outgrowth of cultured CGNs under CNS myelin by lowering the expression of RhoA (Figure2I), which suggested that the roles of ephrinB3, sema4D, and Nogo on inhibiting axon regeneration were independent of one another and antagonizing all these inhibitors after SCI should be much more effective than dealing with single ones. Our subsequent in vivo rat T10 complete transection assay also commendably validated this view.

The early acute phase of SCI lasts from 2 to 48 h following injury, which is mainly characterized by neuron and oligodendrocyte death.[26] The loss of oligodendrocytes results in axonal demyelination and the release of inhibitory molecules. In this study, the recombinant CBD-fused proteins are aiming to neutralize the inhibitory effect of the myelin-derived ephrinB3 and sema4D. As shown in Figure 1G, H, both CBD-EphA4-LBD and CBD-PlexinB1-LBD could sustained release from the collagen scaffold during the early acute phase of SCI. Moreover, rats with T8 complete transect that received transplantation of the collagen scaffold functionalized with CBD-EphA4-LBD, CBD-PlexinB1-LBD, and NEP1-40 showed the largest amount of regenerated axons by NF staining (Figure 6N). This suggested that the collagen scaffold combined with the CBD-fused proteins was an excellent drug-sustained release system for SCI treatments. However, NEP1-40 only contained 40 amino acids. CBD modification might affect the

DOI: 10.1021/acsami.5b03879
ACS Appl. Mater. Interfaces 2015, 7, 13960–13971

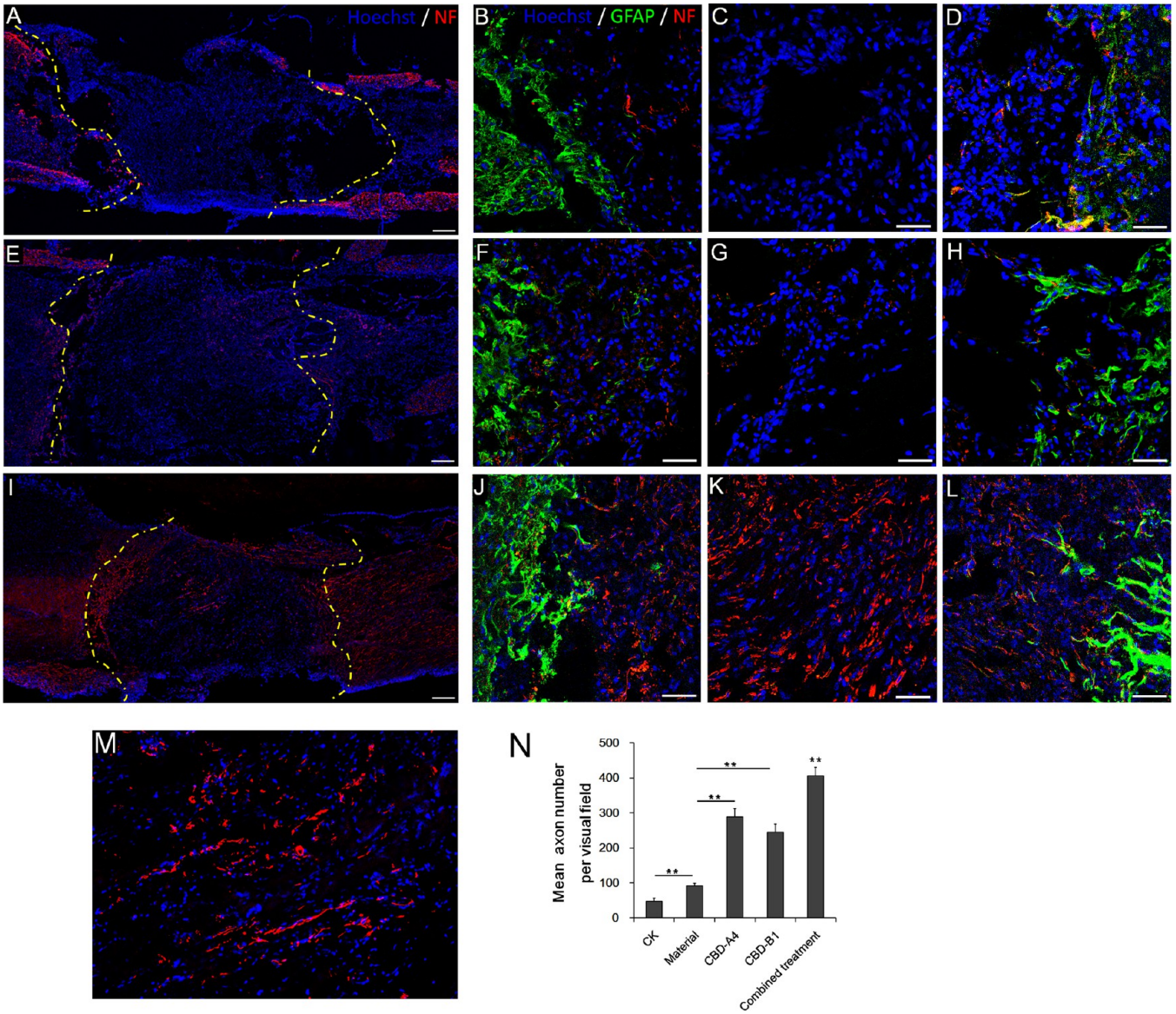

Figure 6. Regenerated axons penetrated out of the GFAP positive border (green) toward the lesion area. (A, E, I) Representative confocal images of animal tissues of groups 1, 2, and 5 at 12 weeks after injury. The full sections showed the density and distance of regenerated NF growth into the lesion sites of animals in different groups; scale bar = 200 μm. (B/C/D, F/G/H, J/K/L) Representative images of the rostral border, caudal border, and the lesion area of A, E, and I, respectively; scale bar = 50 μm. (M) NF-positive fibers penetrated into the lesion area were arranged in order. (N) Quantification of axon number growth into the lesion area 200 μm to the rostral GFAP positive border in groups 1 (CK), 2 (material), 3 (CBD-A4), 4 (CBD-B1), and 5 (combined treatment). *$p < 0.05$ and **$p < 0.01$, determined by one-way ANOVA.

comformation of NEP1-40 to abolish the binding ability to its target. Even though absence of CBD may shorten the acting time of NEP1-40, NEP1-40 could improve the neurite outgrowth in collagen scaffolds in vitro (data not shown). In future work, systemic administration of NEP1-40 would be conducted, which may further improve the regeneration.

Axonal regeneration alone is not sufficient for locomotion recovery. Remyelination of the regenerated axons was considered to be another critical factor during regeneration.[27] The regenerated fibers throughout the lesion area lacking of adequate and proper remyelination might be another reason for poor functional outcome. In this study, 12 weeks after surgery, a transmission electron microscopy study of the regenerated tissues also showed that the myelinated nerve fibers could be found in all groups except group 1 (the blank control). The sickness of the new-formed myelin sheath during groups 2−5 showed no significant difference (Figure 7H, $p < 0.05$). The results indicated that the treatment of the collagen scaffold could support the regeneration of injured axons and their remyelination. However, only attenuating the inhibitory effect of the myelin-associated molecules failed to improve the thickness of the new-formed myelin sheath. Our previous studies found that growth factors such as BDNF could promote the thickness of regenerative myelin,[28] indicating further treatment containing administration of growth factors may led to a better functional outcome.

Locomotor outcomes have been assessed on the BBB scale for 12 weeks after complete T10 transection. Rats in group 5 exhibited significant improvements in the BBB scale compared with group 1 from the first week after surgery until killed ($p < 0.05$; Figure 8). In this study, the spontaneous recovery of hindlimbs locomotor after injury has also been detected

DOI: 10.1021/acsami.5b03879
ACS Appl. Mater. Interfaces 2015, 7, 13960−13971

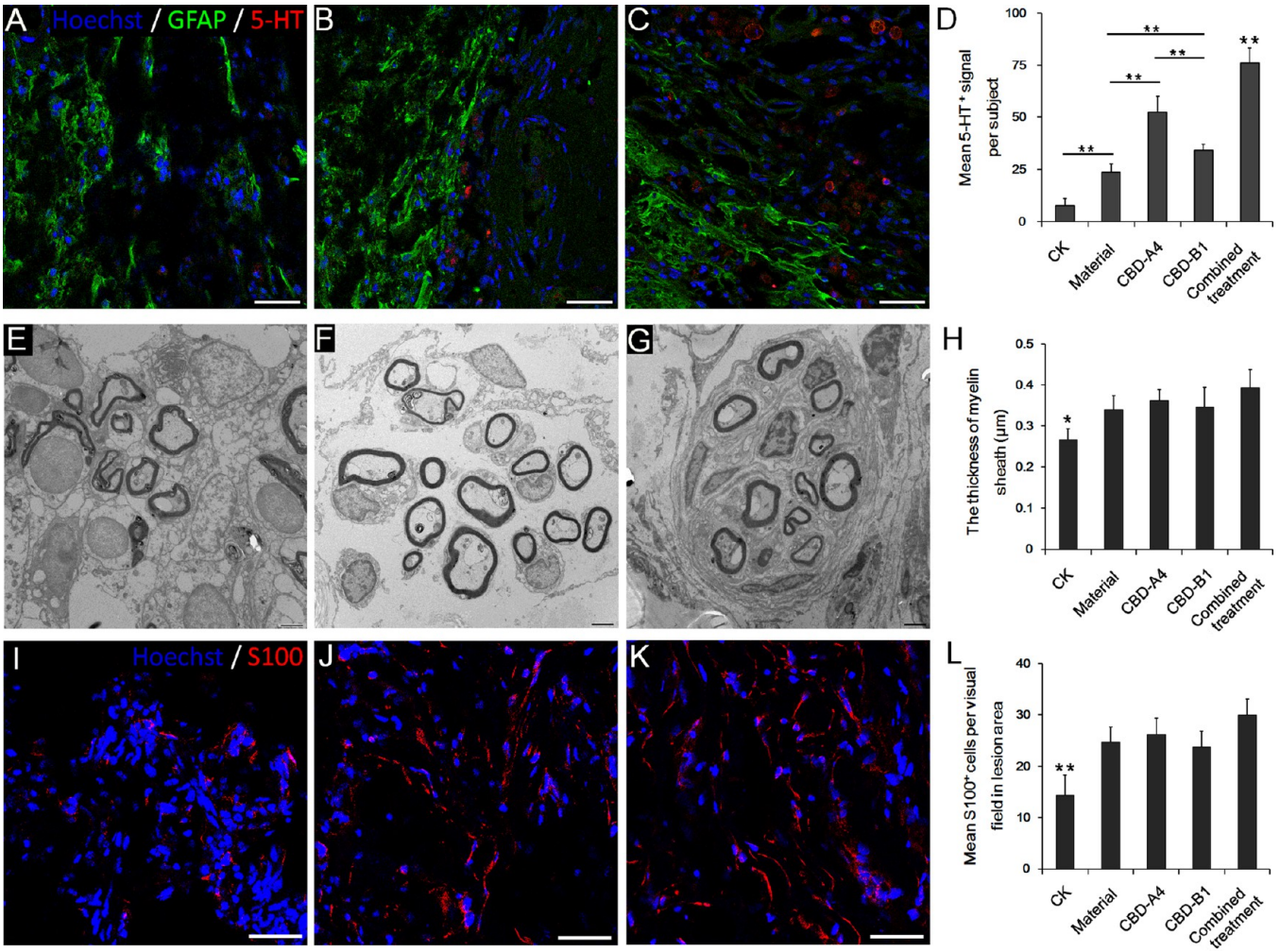

Figure 7. 5-HT-positive neurons, S100-positive cells, and the new-formed myelin sheath in the lesion site. (A–C) Representative confocal images double-labeled of 5-HT (red) and GFAP (green) in groups 1 (A), 2 (B), and 5 (C); scale bars = 50 μm. (D) Quantification of 5-HT-positive signal discovered from the lesion area near to the rostral GFAP positive border in groups 1 (CK), 2 (material), 3 (CBD-A4), 4 (CBD-B1), and 5 (combined treatment). ** $p < 0.01$, determined by one-way ANOVA. (E–G) Representative transmission electron microscopy images showed the myelinated nerve fibers in groups 1 (E), 2 (F), and 5 (G); scale bars = 4 μm. (H) Statistics of the sickness of the new-formed myelin of each group. **$p < 0.01$, determined by one-way ANOVA. (I–K) Representative confocal images of S100 (red) in the lesion area of rats in groups 1 (I), 2 (J), and 5 (K); scale bars = 50 μm. (L) Quantification of the average S100-positive signal per visual field discovered in the lesion area of rats in groups 1–5. ** $p < 0.01$, determined by one-way ANOVA.

without any treatments (group 1); however, BBB scores of animals in group 1 showed very limited rise (only 1–2 points, Figure 8), indicating the spontaneous recovery without any therapy was very limited. As to the transplantation of the functionalized collagen scaffold, combinatorial treatment could recover the function of hindlimbs soon after injury, and the therapeutic effect could last at least in the subsequent three months (Figure 8).

By histological analysis, we found many regenerated axons in group 5 have penetrated both from the rostral and caudal borders into the lesion area and finally reached the caudal border (Figure 6). However, the locomotor outcome of rats in group 5 was not so optimiztic with BBB scores of only 5–6 (Figure 8). The results above indicated that rebuilding of the injured spinal neural connection was much more arduous and complex than we thought, and the possible reasons for this less optimistic outcome might include the following: (1) The absence of the neurotrophic stimulation and protection of growth factors. In our previously studies, we were focusing on the administration of neurotrophic factors alone or in combined with biomaterial scaffolds to the injured spinal cord, and those therapeutic strategies were identified to promote the survival and regeneration of many types of neurons.[17,23,29−32] Therefore, the combined application of neurotrophic factors was the next consideration. (2) Although some long regenerated axons throughout the lesion area could be detected in group 5, the quantity might be not enough for locomotion recovery, and the regenerated axons were likely to inappropriately form contacts with the downstream target. (3) Axonal regeneration alone was not sufficient for locomotion recovery because remyelination of the regenerated axons should be regarded as a critical factor.[27] The regenerated fibers throughout the lesion area lack of adequate and proper remyelination might be another reason for poor functional outcome. (4) Specific rehabilitation strategies might be an important element required for axonal regeneration and locomotion recovery.[33]

DOI: 10.1021/acsami.5b03879
ACS Appl. Mater. Interfaces 2015, 7, 13960−13971

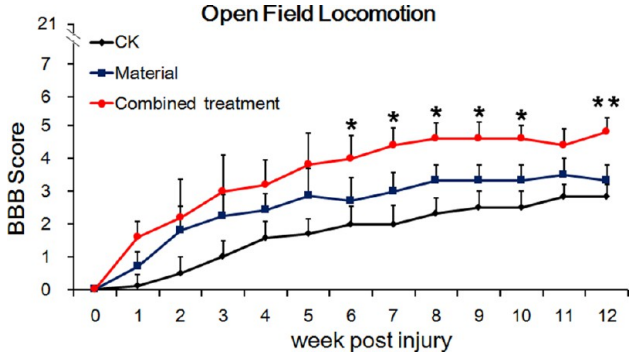

Figure 8. BBB scores of rats in groups 1 (CK, n = 6 until killed), 2 (material, n = 7 until killed), and 5 (combined treatment, n = 10 until killed) from surgery to 12 weeks postinjury. Animals were allowed to assess the movements of hindlimbs weekly by two independent observers blinded to the identity of the treatments. Group 5 showed the highest score among all groups, and the differences between groups 5 and 1 (or 2) were statistically significant from the sixth week postinjury. *p < 0.05, **p < 0.01, determined by one-way ANOVA.

5. CONCLUSIONS

With the continuous deepening understanding of the multi-faced inhibitory nature for axonal regrowth after SCI, the treatment strategies have been developing smoothly.[34] In general, combinatorial therapies were more effective to overcome multiple barriers and provide synergistic effects on locomotion recovery. Given this, we designed a treatment comprehensively dealing with the currently known MAIs responsible for the failing of axonal regeneration on the challenging model of complete spinal cord transection. By embedding in the transplanted collagen scaffold with the collagen-binding proteins that neutralizing the inhibitory molecules Nogo, ephrinB3, and sema4D, we found that the transplantation of functionalized scaffold could effectively facilitate axonal regrowth and remyelination of the regenerated tissue.

AUTHOR INFORMATION

Corresponding Author

*Phone/fax: 86-010-82614426; E-mail: jwdai@genetics.ac.cn.

Author Contributions

‖Xing Li and Jin Han contributed equally to this work.

Notes

The authors declare no competing financial interest.

ACKNOWLEDGMENTS

This work was supported by the "Strategic Priority Research Program of the Chinese Academy of Sciences" (grant no. XDA01030000), the National High Technology Research and Development Program ("863" Program) of China (2012AA020501 and 2013AA020106), the Ministry of Science and Technology of China (2011CB965001 and

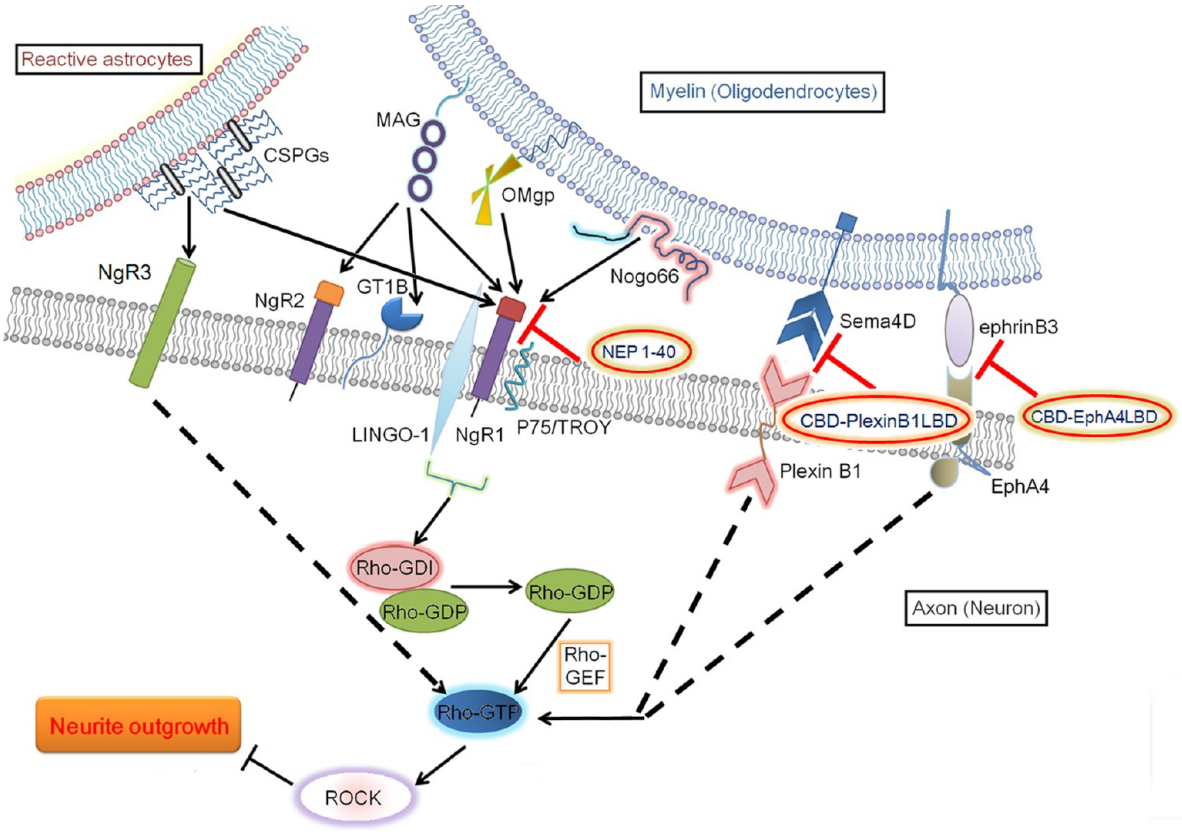

Figure 9. Role and signaling pathway of various inhibitors in axonal regeneration. The failure of SCI regeneration was partly attributed to the presence of myelin-associated or reactive astrocytes-derived inhibitors. The MAIs from myelin debris, including myelin-associated glycoprotein (MAG), Nogo, oligodendrocyte myelin glycoprotein (OMgp), ephrinB3, and the semaphorin4D (sema4D), interact with their respective receptor and exert an inhibition effect of neurite outgrowth by activating Rho. The receptors for glial scar-derived inhibitors chondroitin sulfate proteoglycans (CSPGs) also share some receptors and signaling pathway with MAIs.

DOI: 10.1021/acsami.5b03879
ACS Appl. Mater. Interfaces 2015, 7, 13960−13971

2014CB965003), and the National Science Foundation of China (51361130033).

REFERENCES

(1) Maier, C.; Schwab, E. Sprouting, Regeneration and Circuit Formation in the Injured Spinal Cord: Factors and Activity. *Philos. Trans. R. Soc., B* **2006**, *361* (1473), 1611−1634.
(2) Filbin, T. Recapitulate Development to Promote Axonal Regeneration: Good or Bad Approach? *Philos. Trans. R. Soc., B* **2006**, *361* (1473), 1565−1574.
(3) He, G.; Koprivica, V. The Nogo Signaling Pathway for Regeneration Block. *Annu. Rev. Neurosci.* **2004**, *27*, 341−368.
(4) Fitch, T.; Silver, J. CNS Injury, Glial Scars, and Inflammation: Inhibitory Extracellular Matrices and Regeneration Failure. *Exp. Neurol.* **2008**, *209* (2), 294−301.
(5) Cao, X.; Gao, Y.; Deng, W.; Williams, G.; Doherty, P.; Walsh, S. Receptors for Myelin Inhibitors: Structures and Therapeutic Opportunities. *Mol. Cell Neurosci.* **2010**, *43* (1), 1−14.
(6) Li, X.; Strittmatter, M. Delayed Systemic Nogo-66 Receptor Antagonist Promotes Recovery from Spinal Cord Injury. *J. Neurosci.* **2003**, *23* (10), 4219−4227.
(7) Li, X.; Liu, P.; Budel, S.; Li, W.; Ji, X.; Walus, L.; Li, W.; Jirik, A.; Rabacchi, S.; Choi, E.; Worley, D.; Sah, Y.; Pepinsky, B.; Lee, D.; Relton, J.; Strittmatter, M. Blockade of Nogo-66, Myelin-Associated Glycoprotein, and Oligodendrocyte Myelin Glycoprotein by Soluble Nogo-66 Receptor Promotes Axonal Sprouting and Recovery after Spinal Injury. *J. Neurosci.* **2004**, *24* (46), 10511−10520.
(8) Cao, Y.; Shumsky, S.; Sabol, A.; Kushner, A.; Strittmatter, S.; Hamers, T.; Lee, S.; Rabacchi, A.; Murray, M. Nogo-66 Receptor Antagonist Peptide (NEP1-40) Administration Promotes Functional Recovery and Axonal Growth After Lateral Funiculus Iinjury in the Adult Rat. *Neurorehabil. Neural Repair* **2008**, *22* (3), 262−278.
(9) Benson, D.; Romero, I.; Lush, E.; Lu, R.; Henkemeyer, M.; Parada, F. Ephrin-B3 Is a Myelin-Based Inhibitor of Neurite Uutgrowth. *Proc. Natl. Acad. Sci. U.S.A.* **2005**, *102* (30), 10694−10699.
(10) Duffy, P.; Wang, X.; Siegel, S.; Tu, N.; Henkemeyer, M.; Cafferty, B.; Strittmatter, M. Myelin-Derived EphrinB3 Restricts Axonal Regeneration and Recovery after Adult CNS Injury. *Proc. Natl. Acad. Sci. U.S.A.* **2012**, *109* (13), 5063−8.
(11) Fabes, J.; Anderson, P.; Yanez-Munoz, J.; Thrasher, A.; Brennan, C.; Bolsover, S. Accumulation of the Inhibitory Receptor EphA4 May Prevent Regeneration of Corticospinal Tract Axons Following Lesion. *Eur. J. Neurosci.* **2006**, *23* (7), 1721−1730.
(12) Goldshmit, Y.; Galea, P.; Wise, G.; Bartlett, F.; Turnley, A. Axonal Regeneration and Lack of Astrocytic Gliosis in EphA4-Deficient Mice. *J. Neurosci.* **2004**, *24* (45), 10064−10073.
(13) Moreau-Fauvarque, C.; Kumanogoh, A.; Camand, E.; Jaillard, C.; Barbin, G.; Boquet, I.; Love, C.; Jones, Y.; Kikutani, H.; Lubetzki, C.; Dusart, I.; Chedotal, A. The Transmembrane Semaphorin Sema4D/CD100, an Inhibitor of Axonal Growth, Is Expressed on Oligodendrocytes and Upregulated after CNS Lesion. *J. Neurosci.* **2003**, *23* (27), 9229−9239.
(14) Zhang, L.; Wang, J.; Tang, L. Sema4D Knockdown in Oligodendrocytes Promotes Functional Recovery after Spinal Cord Injury. *Cell Biochem. Biophys.* **2014**, *68* (3), 489−96.
(15) Lu, P.; Tuszynski, H. Growth Factors and Combinatorial Therapies for CNS Regeneration. *Exp. Neurol.* **2008**, *209* (2), 313−320.
(16) Han, Q.; Sun, J.; Lin, H.; Zhao, X.; Gao, Y.; Zhao, N.; Chen, B.; Xiao, F.; Hu, W.; Li, Y.; Yang, B.; Dai, W. Linear Ordered Collagen Scaffolds Loaded with Collagen-Binding Brain-Derived Neurotrophic Factor Improve the Recovery of Spinal Cord Injury in Rats. *Tissue Eng., Part A* **2009**, *15* (10), 2927−2935.
(17) Han, Q.; Jin, W.; Xiao, F.; Ni, B.; Wang, H.; Kong, J.; Wu, J.; Liang, B.; Chen, L.; Zhao, N.; Chen, B.; Dai, W. The Promotion of Neural Regeneration in an Extreme Rat Spinal Cord Injury Model Using a Collagen Scaffold Containing a Collagen Binding Neuroprotective Protein and an EGFR Neutralizing Antibody. *Biomaterials* **2010**, *31* (35), 9212−9220.
(18) Liang, B.; Han, Q.; Jin, W.; Xiao, F.; Huang, C.; Ni, B.; Chen, B.; Kong, J.; Wu, J.; Dai, W. The Promotion of Neurological Recovery in the Rat Spinal Cord Crushed Injury Model by Collagen-Binding BDNF. *Biomaterials* **2010**, *31* (33), 8634−8641.
(19) Fan, J.; Xiao, F.; Zhang, T.; Chen, B.; Tang, Q.; Hou, L.; Ding, Y.; Wang, B.; Zhang, P.; Dai, W.; Xu, X. Linear Ordered Collagen Scaffolds Loaded with Collagen-Binding Neurotrophin-3 Promote Axonal Regeneration and Partial Functional Recovery after Complete Spinal Cord Transection. *J. Neurotrauma* **2010**, *27* (9), 1671−1683.
(20) Wang, B.; Xiao, F.; Chen, B.; Han, J.; Gao, Y.; Zhang, J.; Zhao, X.; Wang, X.; Dai, W. Nogo-66 Promotes the Differentiation of Neural Progenitors into Astroglial Lineage Cells through mTOR-STAT3 Pathway. *PLoS One* **2008**, *3* (3), e1856.
(21) Chen, L.; Xiao, F.; Meng, Y.; Zhao, N.; Han, J.; Su, N.; Chen, B.; Dai, W. The Enhancement of Cancer Stem Cell Properties of MCF-7 Cells in 3D Collagen Scaffolds for Modeling of Cancer and Anticancer Drugs. *Biomaterials* **2012**, *33* (5), 1437−1444.
(22) Bilimoria, P. M.; Bonni, A. Cultures of Cerebellar Granule Neurons. *Cold Spring Harbor Protoc.* **2008**, *3* (12), 1−7 DOI: 10.1101/pdb.prot5107.
(23) Fan, J.; Zhang, T.; He, H.; Xiao, F.; Chen, B.; Xiaodan, A.; Dai, W.; Xu, X. Neural Regrowth Induced by PLGA Nerve Conduits and Neurotrophin-3 in Rats with Complete Spinal Cord Transection. *J. Biomed. Mater. Res., Part B* **2011**, *97B* (2), 271−277.
(24) Basso, M.; Beattie, S.; Bresnahan, C. Graded Histological and Locomotor Outcomes after Spinal Cord Contusion Using the NYU Weight-Drop Device Versus Transection. *Exp. Neurol.* **1996**, *139* (2), 244−256.
(25) Egea, J.; Klein, R. Bidirectional Eph-ephrin Signaling during Axon Guidance. *Trends Cell Biol.* **2007**, *17* (5), 230−8.
(26) Rowland, W.; Hawryluk, W. J.; Kwon, B.; Fehlings, G. Current Status of Acute Spinal Cord Injury Pathophysiology and Emerging Therapies: Promise on the Horizon. *Neurosurg. Focus* **2008**, *25* (5), E2.
(27) Alto, T.; Havton, A.; Conner, M.; Hollis, R.; Blesch, A.; Tuszynski, H. Chemotropic Guidance Facilitates Axonal Regeneration and Synapse Formation after Spinal Cord Injury. *Nat. Neurosci.* **2009**, *12* (9), 1106−U8.
(28) Han, S.; Wang, B.; Jin, W.; Xiao, Z.; Li, X.; Ding, W.; Kapur, M.; Chen, B.; Yuan, B.; Zhu, T.; Wang, H.; Wang, J.; Dong, Q.; Liang, W.; Dai, J. The Linear-Ordered Collagen Scaffold-BDNF Complex Significantly Promotes Functional Recovery after Completely Transected Spinal Cord Iinjury in Canine. *Biomaterials* **2015**, *41*, 89−96.
(29) Kadoya, K.; Tsukada, S.; Lu, P.; Coppola, G.; Geschwind, D.; Filbin, M. T.; Blesch, A.; Tuszynski, M. H. Combined Intrinsic and Extrinsic Neuronal Mechanisms Facilitate Bridging Axonal Regeneration One Year after Spinal Cord Injury. *Neuron* **2009**, *64* (2), 165−172.
(30) Lu, P.; Blesch, A.; Graham, L.; Wang, Y. Z.; Samara, R.; Banos, K.; Haringer, V.; Havton, L.; Weishaupt, N.; Bennett, D.; Fouad, K.; Tuszynski, M. H. Motor Axonal Regeneration after Partial and Complete Spinal Cord Transection. *J. Neurosci.* **2012**, *32* (24), 8208−8218.
(31) Lu, P.; Wang, Z.; Graham, L.; McHale, K.; Gao, Y.; Wu, D.; Brock, J.; Blesch, A.; Rosenzweig, S.; Havton, A.; Zheng, H.; Conner, M.; Marsala, M.; Tuszynski, H. Long-Distance Growth and Connectivity of Neural Stem Cells after Severe Spinal Cord Injury. *Cell* **2012**, *150* (6), 1264−1273.
(32) Li, R.; Xiao, F.; Han, J.; Chen, L.; Xiao, S.; Ma, K.; Hou, L.; Li, X.; Sun, J.; Ding, Y.; Zhao, N.; Chen, B.; Dai, W. Promotion of Neuronal Differentiation of Neural Progenitor Cells by Using EGFR Antibody Functionalized Collagen Scaffolds for Spinal Cord Injury Repair. *Biomaterials* **2013**, *34* (21), 5107−5116.
(33) Garcia-Alias, G.; Barkhuysen, S.; Buckle, M.; Fawcett, J. W.; Chondroitinase, A. B. C. Treatment Opens a Window of Opportunity for Task-Specific Rehabilitation. *Nat. Neurosci.* **2009**, *12* (9), 1145−U16.
(34) McCreedy, A.; Sakiyama-Elbert, E. Combination Therapies in the CNS: Engineering the Environment. *Neurosci. Lett.* **2012**, *519* (2), 115−121.

DOI: 10.1021/acsami.5b03879
ACS Appl. Mater. Interfaces 2015, 7, 13960−13971